



Article

Synthesis and Self-Assembled Behavior of pH-Responsive Chiral Liquid Crystal Amphiphilic Copolymers Based on Diosgenyl-Functionalized Aliphatic Polycarbonate

Zhi-Hao Guo ¹, Xiao-Feng Liu ¹, Jian-She Hu ^{1,*}, Li-Qun Yang ² and Zhang-Pei Chen ¹

¹ Center for Molecular Science and Engineering, College of Science, Northeastern University, Shenyang 110819, China; 1610046@stu.neu.edu.cn (Z.-H.G.); 1510048@stu.neu.edu.cn (X.-F.L.); chenzhangpei@mail.neu.edu.cn (Z.-P.C.)

² Key Laboratory of Reproductive Health and Medical Genetics, National Health and Family Planning Commission, Shenyang 110031, China; yanglq@lnszjk.com.cn

* Correspondence: hujs@mail.neu.edu.cn; Tel.: +86-024-8368-7671

Received: 22 May 2017; Accepted: 30 June 2017; Published: 4 July 2017

Abstract: The morphological control of polymer micellar aggregates is an important issue in applications such as nanomedicine and material science. Stimuli responsive soft materials have attracted significant attention for their well-controlled morphologies. However, despite extensive studies, it is still a challenge to prepare nanoscale assemblies with responsive behaviors. Herein, a new chiral liquid crystal (LC) aliphatic polycarbonate with side chain bearing diosgenyl mesogen, named mPEG₄₃-PMCC₂₅-P(MCC-DHO)₁₅, was synthesized through the ring-opening polymerization and coupling reaction. The self-assembled behavior of the LC copolymer was explored. In aqueous solution, the functionalized copolymer could self-organize into different nanostructures with changing pH value, such as nanospheres and nanofibers. This would offer new possibilities in the design of nanostructured organic materials.

Keywords: diosgenin; liquid crystal; self-assembly; nanospheres; nanofibers

1. Introduction

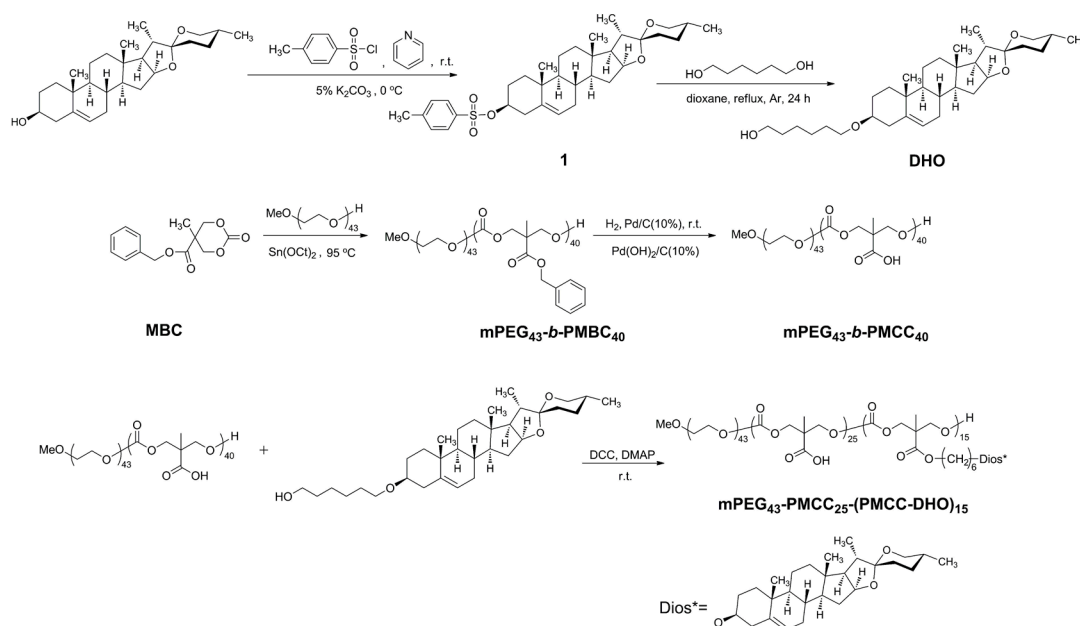
Self-assembled amphipathic polymers have wide applications in nanomedicine and material science. In mixed solvent and driven by hydrophobic chains, self-assembly of amphipathic macromolecular forms stable aggregates with hydrophobic chain as core and hydrophilic chain as shell. Recent research has indicated that the amphiphilic block copolymer reveals a controlled balance of amphiphilicity and can assume various well-organized architectures, such as spherical, rodlike, vesicles and lamellar structures, etc. [1–7]. In general, the morphologies and sizes of polymer micellar aggregates can be designed through molecular weight selection [8–10], chain architecture design [11–13], degree of crosslinking [6,14] and variation of solution conditions [1,15–24]. So, a variety of smart nanomaterial systems are constructed by association of various kinds of amphipathic polymers, including proteins, DNA, and phospholipids, through well-controlled self-assembly [25,26].

Chiral liquid crystal (LC) materials attracts considerable attention due to their excellent optical-electric properties, such as selective reflection of circular polarized light, high optical rotatory power, circular dichroism, thermochromism, ferroelectricity and piezoelectricity [27]. In addition, chiral LC compounds are responsive to external stimuli, such as temperature, pressure, electromagnetic field, etc. Within this context and due to the unique properties, chiral steroidal compounds have become an important part of smart materials. Stupp et al. [28] first reported the synthesis of cholesterol end functionalized oligo(L-lactic acid) and its interaction with cells. Subsequently, Guo [29] and

Cheng et al. [30] reported cholesteryl end-capped aliphatic polycarbonates and dicholesteryl end functionalized triblock poly(ϵ -caprolactone), respectively, as biodegradable polymers. Recently, the cholesteryl-functional polymers have been applied in the field of nanomedicine, such as drugs or nucleic acids delivery, complex hydrophobic therapeutics, etc. [31].

Diosgenin, an important kind of chiral steroidal compounds extracted from *dioscorea zingiberensis*, was used to synthesize sex hormones, steroids, and so on [32–35]. Some studies have revealed that diosgenin has multiple biological activities, such as anti-infection [36,37], anti-thrombus [38], enhancing immune activity of T-cells [39], and inhibition of cancer cell proliferation [40]. The diosgenin and its derivatives can be used as bioactive LC functional mesogens for their good biocompatibility. In addition, to the best of our knowledge, although biodegradable copolymers containing side active groups for the drug delivery has been studied [41,42], few research on the biodegradable aliphatic polycarbonate containing side diosgenyl groups as biomesogenic units is reported. Therefore, it's an interesting research on synthesizing biodegradable side chain chiral LC polycarbonate derived from diosgenin, studying their self-assembled behavior and exploring the potential applications in the field of biomedical science, such as drug delivery and tissue engineering templates.

Hence, on the basis of the above consideration, a new chiral LC polycarbonate with side chain bearing diosgenyl mesogen, named as $mPEG_{43}$ -PMCC₂₅-P(MCC-DHO)₁₅, is synthesized through the ring-opening polymerization and coupling reaction (Scheme 1). A side chain functionalized diosgenin with hydrophobic moiety is incorporated onto the aliphatic polycarbonate for the introduction of physicochemical functionality such as mesomorphism. Furthermore, due to the existence of the multifunctional diosgenyl, the properties of $mPEG_{43}$ -PMCC₂₅-P(MCC-DHO)₁₅ such as phase behavior and self-assembled behavior are studied.



Scheme 1. Synthetic route to copolymer.

2. Results and Discussion

2.1. Synthesis and Structural Characterization of $mPEG_{43}$ -b-PMBC₄₀

For the preparation of aliphatic polycarbonates the ring-opening polymerization is an efficient method. In general, the ring-opening polymerization of aliphatic cyclic carbonate monomer could be carried out in the presence of an initiator with hydroxyl groups such as mPEG. In this study, 5-methyl-5-benzoyloxycarbonyl-1,3-dioxan-2-one (MBC) was first obtained by a previously reported procedure with a slight modification [43], proton nuclear magnetic resonance (¹H NMR) spectra of

MBC is shown as Figure S1. Then $m\text{PEG}_{43}\text{-}b\text{-PMBC}_{40}$ was synthesized through the ring-opening polymerization of the functionalized cyclic carbonate monomer MBC using $\text{Sn}(\text{Oct})_2$ as a catalyst in the presence of $m\text{PEG}_{43}$ as a macroinitiator. The ring-opening polymerization was confirmed by ^1H NMR spectra (Figure S2), Fourier transform infrared (FT-IR) spectroscopy (Figure S3) and gel permeation chromatographic (GPC) (Figure S4) analysis. After the ring-opening polymerization, the corresponding signals of methylene proton in the cyclic monomer MBC at 4.69 and 4.19 ppm shifted to 4.29 ppm. Compared with the $\text{C}=\text{O}$ stretching vibration bands of MBC at 1752 and 1737 cm^{-1} , the $\nu(\text{C}=\text{O})$ of $m\text{PEG}_{43}\text{-}b\text{-PMBC}_{40}$ only appeared a peak at 1754 cm^{-1} . The GPC analysis confirmed the degree of polymerization and dispersity of the aliphatic polycarbonates, and indicated that the monomer reacted completely.

2.2. Synthesis and Structural Characterization of $m\text{PEG}_{43}\text{-}b\text{-PMCC}_{40}$

The preparation of $m\text{PEG}_{43}\text{-}b\text{-PMCC}_{40}$ was carried out by construction of a polycarbonate containing one reactive side chain carboxylic acid functionality at each repeat unit. $m\text{PEG}_{43}\text{-}b\text{-PMCC}_{40}$ was obtained by hydrogenolysis reaction to result in the deprotection of side benzyl groups for $m\text{PEG}_{43}\text{-}b\text{-PBMC}_{40}$ using H_2 gas, Pd/C and $\text{Pd}(\text{OH})_2/\text{C}$ as co-catalysts. The cleavage of the benzyl ester groups was confirmed by ^1H NMR (Figure S5) and FT-IR (Figure S3) spectroscopy. Compared with the ^1H NMR of $m\text{PEG}_{43}\text{-}b\text{-PBMC}_{40}$, the proton signals of the benzyl groups at 7.35–7.28 and 5.14 ppm disappeared for $m\text{PEG}_{43}\text{-}b\text{-PMCC}_{40}$, in addition, the FT-IR spectroscopy of $m\text{PEG}_{43}\text{-}b\text{-PMCC}_{40}$ appeared typical peak of carboxyl group at $3600\text{--}2500\text{ cm}^{-1}$, which indicated that the elimination of the benzyl groups was complete.

2.3. Synthesis and Structural Characterization of $m\text{PEG}_{43}\text{-PMCC}_{25}\text{-P}(\text{MCC-DHO})_{15}$

The availability of pendant diosgenyl groups for further functionalization was demonstrated by an esterification reaction between $m\text{PEG}_{43}\text{-}b\text{-PMCC}_{40}$ and 6-diosgenoxyhexane-1-ol (DHO) using DCC as a coupling agent and DMAP as a catalyst. The formation of ester bonds was confirmed by a shift of the methane ($\text{HOCH}_2\text{-}$) peak from 3.65 ppm in DHO to 4.12 ppm in $m\text{PEG}_{43}\text{-PMCC}_{25}\text{-P}(\text{MCC-DHO})_{15}$, the number of DHO was determined by the integration values ratio of the proton signals at 4.12 for $\text{O}=\text{COCH}_2\text{-}$ to 3.65 for CH_2 in $m\text{PEG}_{43}$. Figure 1 shows the ^1H NMR spectra of $m\text{PEG}_{43}\text{-PMCC}_{25}\text{-P}(\text{MCC-DHO})_{15}$. In addition, the $\nu(\text{-COOH})$ at $3600\text{--}2500\text{ cm}^{-1}$ for $m\text{PEG}_{43}\text{-}b\text{-PMCC}_{40}$ were not obvious, these results showed that the diosgenyl groups were successfully introduced to side chain of the aliphatic polycarbonates.

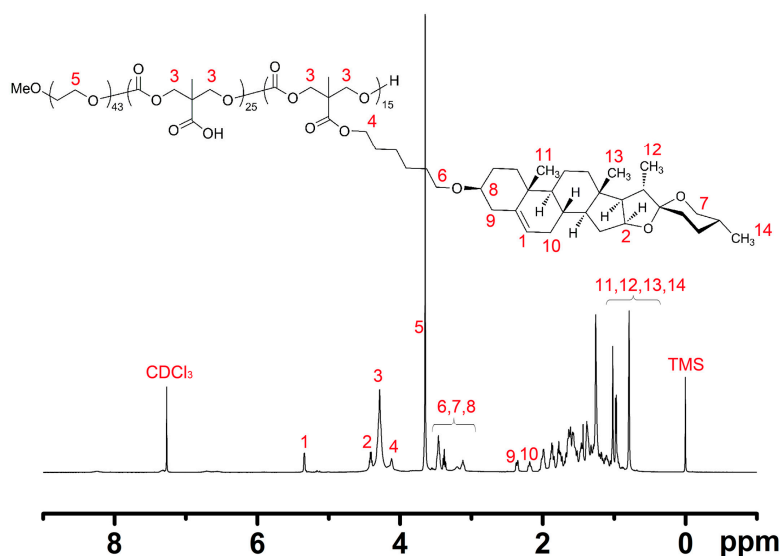


Figure 1. ^1H NMR spectra of $m\text{PEG}_{43}\text{-PMCC}_{25}\text{-P}(\text{MCC-DHO})_{15}$.

2.4. Liquid Crystal Behaviour of $m\text{PEG}_{43}\text{-PMCC}_{25}\text{-P(MCC-DHO)}_{15}$

From a scientific and commercial point of view, chiral LC materials with helical supramolecular structure are fascinating. As known, chirality can be introduced into LC molecules at various levels, and is usually located in the terminal position of the mesogenic core. The rod-like, chiral molecules responsible for the macroscopical alignment of the mesogenic domains can produce cholesteric or a chiral smectic phase. The LC behaviour of $m\text{PEG}_{43}\text{-PMCC}_{25}\text{-P(MCC-DHO)}_{15}$ was investigated with differential scanning calorimetry (DSC), X-ray diffraction (XRD) and polarizing optical microscopy (POM). According to DSC heating curve, a typical glass transition appeared indicating that the LC copolymer was amorphous polymer (Shown in Figure 2a). In addition, $m\text{PEG}_{43}\text{-PMCC}_{25}\text{-P(MCC-DHO)}_{15}$ exhibited a mesomorphism to isotropic phase transition at $105.0\text{ }^{\circ}\text{C}$ because the mesogenic DHO units were introduced to side-chain of the polycarbonate. POM observations showed that $m\text{PEG}_{43}\text{-PMCC}_{25}\text{-P(MCC-DHO)}_{15}$ exhibited obvious mesomorphism at body temperature ($\approx 37\text{ }^{\circ}\text{C}$). When the temperature increased to $116.9\text{ }^{\circ}\text{C}$, the birefringence disappeared. To further identify mesophase structure, variable-temperature XRD studies were carried out. Figure 2b shows the XRD patterns of $m\text{PEG}_{43}\text{-PMCC}_{25}\text{-P(MCC-DHO)}_{15}$ at $100\text{ }^{\circ}\text{C}$, only a weak and diffuse peak at wide angle was observed, indicating the formation of a cholesteric phase.

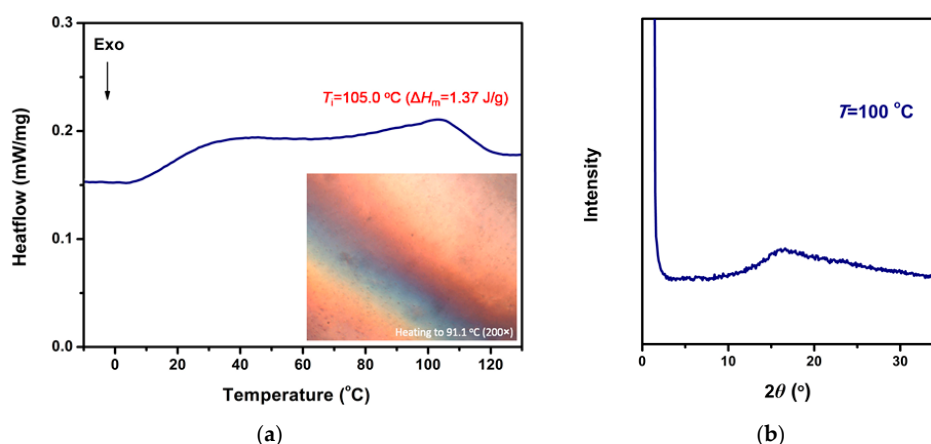


Figure 2. (a) Differential scanning calorimetry (DSC) curves of $m\text{PEG}_{43}\text{-PMCC}_{25}\text{-P(MCC-DHO)}_{15}$, the inset at lower right is photograph on heating to $91.1\text{ }^{\circ}\text{C}$ recorded by polarizing optical microscopy (POM); (b) X-ray diffraction (XRD) curve of $m\text{PEG}_{43}\text{-PMCC}_{25}\text{-P(MCC-DHO)}_{15}$ at $100\text{ }^{\circ}\text{C}$.

2.5. pH Responsive Self-Assembly of $m\text{PEG}_{43}\text{-PMCC}_{25}\text{-P(MCC-DHO)}_{15}$

The morphologies of $m\text{PEG}_{43}\text{-PMCC}_{25}\text{-P(MCC-DHO)}_{15}$ nano-aggregates were analyzed by scanning electron microscopes (SEM) and transmission electron microscopy (TEM). SEM images of the aggregates are shown in Figure 3. An interesting phenomenon was that the micellar aggregates in water could show different pH-responsive morphologies including spherical and nanofibers aggregates. In acidic conditions ($\text{pH} < 7.0$), the morphology of aggregates exhibited nanospheres (Figure 3A,B), however, when the pH increased to 7.0, the nanospheres began to stretch to nanofibers, and a few spherical structures (average radius of spheres: 115.1 nm) were still visible (Figure 3C). Fortunately, the clear transition process of nanospheres to nanofibers was observed at $\text{pH} = 8.0$ (Figure 3D). To further confirm the existence of the morphologies in $m\text{PEG}_{43}\text{-PMCC}_{25}\text{-P(MCC-DHO)}_{15}$ sample, it was subjected to a transmission electron microscope (TEM) (Figure S6), the images given a significant evidence that the micellar aggregates were solid rather than hollow. When $\text{pH} < 7.0$, the nanospheres could merge with others, as shown in the Figure 3A,B, this phenomenon led that the sizes of the most aggregates were larger than the practical sizes, therefore, the minimum size of the spherical aggregates recorded by electron microscopes was the nearest to their actual size. Similarly, the nanofibers could also merge into others and large diameter nanofibers formed.

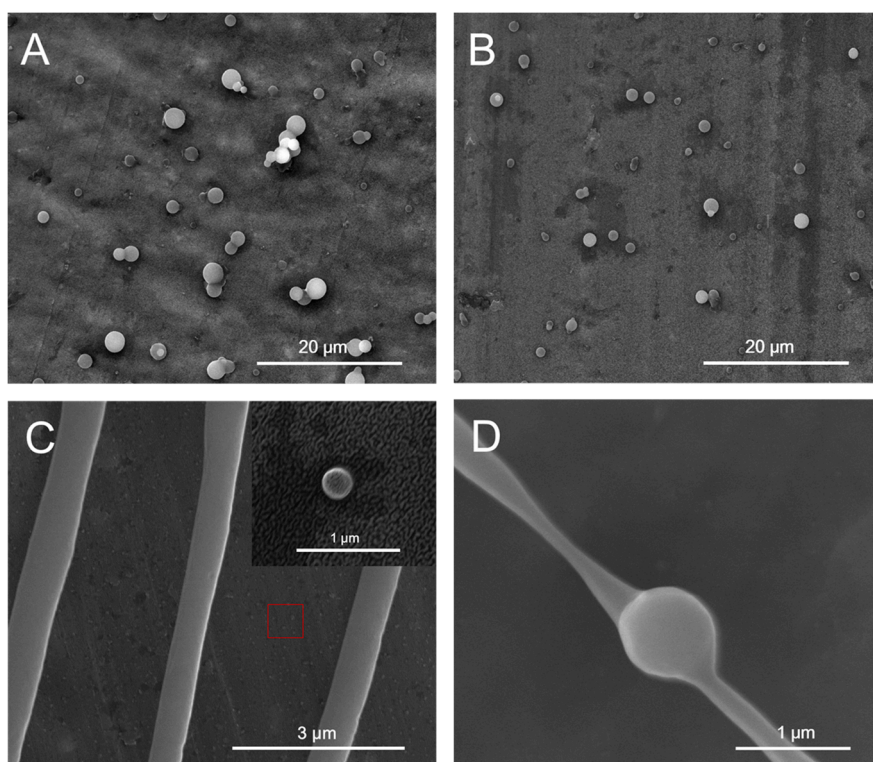


Figure 3. SEM images of $m\text{PEG}_{43}\text{-PMCC}_{25}\text{-P(MCC-DHO)}_{15}$ self-assembly obtained in water at (A) pH = 4.0, (B) pH = 6.0, (C) pH = 7.0 and (D) pH = 8.0. The inset at higher right in (C) is an enlargement of the spherical aggregates in the selected rectangular area.

To trace structural changes in the spherical assemblies, the sizes of the aggregates were also measured by DLS with changing pH value. DLS histograms of $m\text{PEG}_{43}\text{-PMCC}_{25}\text{-P(MCC-DHO)}_{15}$ at pH = 2.0 and 6.0 are shown as Figure 4a,b, and the effect of pH value on the sizes of aggregates is shown as Figure 4c. When pH = 2.0, average radius of the spherical assemblies was 327.3 nm (PDI = 0.039), with increasing pH value to 6.0, the radius of nanospheres decreased to 232.0 nm (PDI = 0.037). This interesting change provides significant evidence that the spherical assemblies were in response to pH.

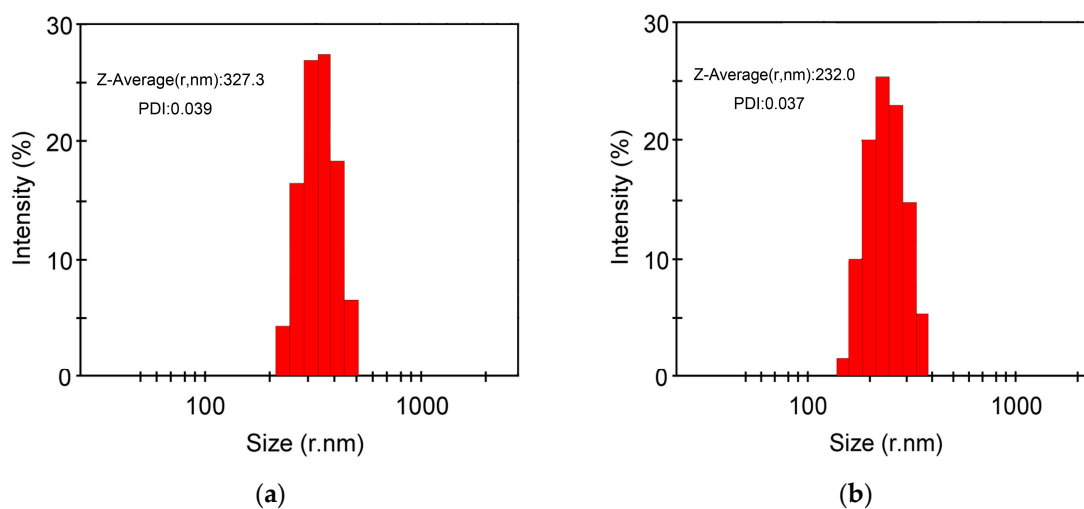


Figure 4. Cont.

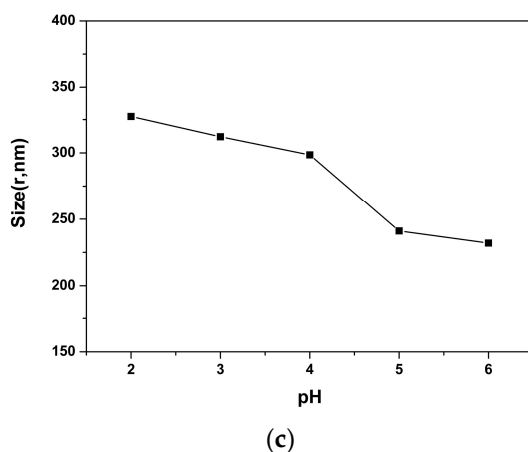


Figure 4. Dynamic light scattering (DLS) histogram of mPEG₄₃-PMCC₂₅-P(MCC-DHO)₁₅ in water at (a) pH = 2.0 and (b) pH = 6.0, (c) size of mPEG₄₃-PMCC₂₅-P(MCC-DHO)₁₅ in various pH at 25 °C.

As known, LC materials have good self-organization orientational behavior [44–46]. The ability of side diosgenyl groups to form mesophase will be anticipated to provide an ordered structure for the intermolecular self-assembly. With the incorporation of the mesogen, the movement and arrangement of the amphiphilic aliphatic polycarbonates were influenced by ordered mesophase. In tetrahydrofuran (THF), the macromolecular chain of mPEG₄₃-PMCC₂₅-P(MCC-DHO)₁₅ completely stretched, with dialyzing against selective solvent water, the side diosgenyl groups rearranged and formed ordered mesophase structure, and the hydrophobic segments were frozen in the meanwhile, then, the macromolecular chain collapsed, and the core-shell structure was formed with hydrophobic chain as core and hydrophilic chain as shell (Figure 5). In acidic conditions (pH < 7.0), the nanospheres merged with others and stable aggregates were formed. However, as increasing pH value, the carboxyl groups of mPEG₄₃-PMCC₂₅-P(MCC-DHO)₁₅ tend to ionize to stabilize the aggregates [47], which made the merging process difficult due to the electrostatic repulsions, and the decreasing radius of nanospheres. When pH ≥ 7.0, the nanospheres were highly charged and the strong repulsive electrostatic interactions provided a driving force for stretching the core-shell structure, which in turn influenced the chain conformation from compact nanospheres at low pH to extended nanofibers at high pH.

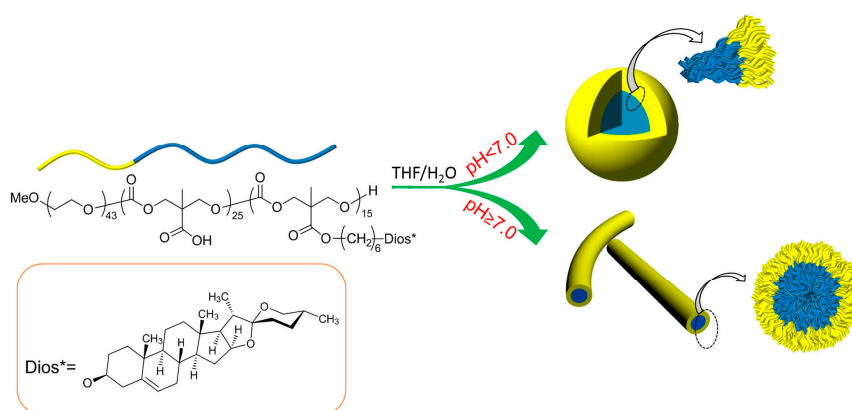


Figure 5. Self-assembly of mPEG₄₃-PMCC₂₅-P(MCC-DHO)₁₅ with nanospheres and nanofibers micelles.

3. Materials and Methods

Tosyl chloride, palladium 10% on carbon, palladium hydroxide, and stannous octoate were purchased from Sinopharm Chemical Reagent Co., Ltd. (Shenyang, China). Diosgenin was

purchased from Wuhan Chemical Industry Co., Ltd. (Wuhan, China). 1,6-Hexanediol was purchased from Qingdao Lilai Fine Chemical Industry Co., Ltd. (Qingdao, China). 5-methyl-5-benzyloxycarbonyl-1,3-dioxan-2-one (MBC) were synthesized as reported [43]. All solvents and reagents used in this study were purified with standard methods.

FT-IR spectra were recorded as a KBr disk on a PerkinElmer spectrum One (B) spectrometer (PerkinElmer, Foster City, CA, USA). ^1H NMR spectra were measured using a Bruker ARX 600 (Bruker, Karlsruhe, Germany) high-resolution NMR spectrometer, and chemical shifts were reported in parts per million with tetramethylsilane (TMS) as an internal standard. Average molecular weights of the polymers were characterized with gel permeation chromatographic (GPC) measurements at room temperature on a Waters 1515 instrument (Waters, Milford, MA, USA) calibrated with a polystyrene standard, and using THF as an eluent. The thermal behavior was determined with a Netzsch 204 (Netzsch, Hanau, Germany) differential scanning calorimetry (DSC) equipped with a cooling system at a heating and cooling rate of $10\text{ }^\circ\text{C}/\text{min}$ in a nitrogen atmosphere. The mesomorphism and phase transition temperature were observed with a Leica DMRX (Leica, Wetzlar, Germany) polarizing optical microscopy (POM) equipped with a Linkam THMSE-600 (Linkam, London, UK) cool and hot stage. X-ray diffraction (XRD) measurements were performed with a nick-filtered $\text{Cu-K}\alpha$ radiation with a Bruker D8 Advance (Bruker, Karlsruhe, Germany) power diffractometer. Dynamic light scattering (DLS) measurements were carried out using a Zetasizer Nano ZS/ZEN3690 (Malvern, England) for the analysis of block copolymer aggregates hydrodynamic radii in a dilute solution. A backscattering measurement angle of 173° was used, repeating the measurement three times for each sample, with 12–15 runs per measurement. Scanning electron microscope (SEM) measurements were performed on an Inspect F50 (FEI., Hillsboro, OR, USA). The samples for SEM observations were prepared by depositing several drops of the samples suspension onto the surface of cleaned aluminum foil, and the samples were quenched by liquid nitrogen, then freeze-dried in vacuum at $-50\text{ }^\circ\text{C}$ for 24 h. The samples were coated with a thin film of gold before measuring. For transmission electron microscopy (TEM), the samples suspension was deposited onto a carbon-coated copper TEM grid and flash-frozen in liquid nitrogen, then freeze-dried in vacuum at $-50\text{ }^\circ\text{C}$ for 24 h. The frozen sample was scanned at 120 kV (JEM-2100, JEOL Ltd., Tokyo, Japan), the size of the particles was measured manually.

Synthesis of DHO. The compound **1** was obtained by reacting diosgenin and tosyl chloride using pyridine as solvent. Then, put compound **1** (14.2 g, 25 mmol), 1,6-hexanediol (59 g, 0.5 mol), and anhydrous 1,4-dioxane (300 mL) in a 500 mL three-neck flask with a magnetic stir bar. After the reaction mixture was refluxed for 24 h under an argon atmosphere, then concentrated under reduced pressure, the residue was dissolved in 100 mL of ethyl acetate. The resulting solution was washed three times with water to remove 1,6-hexanediol, the combined organic layer was dried over anhydrous magnesium sulfate, and then filtered. The filtrate was evaporated to dryness and the crude product was purified by silica gel column chromatography (petroleum ether/ethyl acetate = 3:1) and dried in a vacuum to result in a white powder. FT-IR (KBr, cm^{-1}): 3368 (–OH); 2948, 2868 (CH_3 –, $-\text{CH}_2$ –); 1242, 1096 (C–O–C). ^1H NMR (600 MHz, CDCl_3 , δ , ppm): 5.35 (d, 1H, $J = 6.0\text{ Hz}$, $-\text{CH}=\text{C}<$), 4.41 (q, 1H, $J = 7.8\text{ Hz}$, $<\text{CHO}-$), 3.65 (t, 2H, $J = 6.6\text{ Hz}$, HOCH_2 –), 3.49–3.38 [m, 4H, $\text{HO}(\text{CH}_2)_5\text{CH}_2\text{O}-$ and $-\text{OCH}_2\text{CH}<$], 3.12 [m, 1H, $\text{HO}(\text{CH}_2)_6\text{OCH}<$], 2.37–0.79 [m, 45H, H -diosgenyl and $-(\text{CH}_2)_4$ –]. ^{13}C NMR (600 MHz, CDCl_3 , δ , ppm): 140.67, 121.20, 109.15, 80.70, 79.10, 71.38, 67.85, 66.70, 62.09, 56.41, 49.97, 46.45, 41.48, 40.14, 39.67, 38.88, 37.13, 37.03, 31.96, 31.72, 31.46, 31.29, 30.29, 30.02, 28.78, 28.54, 28.41, 25.82, 20.74, 19.30, 17.05, 16.18, 14.43.

Synthesis of mPEG₄₃-b-PMBC₄₀. MBC (20.0 g, 0.08 mol), mPEG₄₃ (3.8 g, 2.0 mmol), and $\text{Sn}(\text{Oct})_2$ toluene solution (1.62 mL, 0.123 mol/L) were transferred into a glass polymerization flask, then the flask was sealed under vacuum. After the mixture was reacted for 24 h at $95\text{ }^\circ\text{C}$ in an oil bath, the polymer was precipitated in ice-cold methanol (400 mL). Then, the crude polymer was redissolved in dichloromethane and reprecipitated again in ice-cold methanol. The polymer was dried in a vacuum until a constant sample mass was obtained. $M_n^{\text{NMR}} = 11,900\text{ g/mol}$; $M_n^{\text{GPC,THF}} = 9630\text{ g/mol}$; $\text{PDI}^{\text{THF}} = 1.62$. FT-IR (KBr, cm^{-1}): 2974, 2883 (CH_3 –, $-\text{CH}_2$ –); 1754 (C=O); 1498 (Ar–); 1246, 1140

(C–O–C). ^1H NMR (600 MHz, CDCl_3 , δ , ppm): 7.35–7.28 (Ar–H), 5.14 (Ar CH_2O), 4.29 (CH_2 in polycarbonate chain), 3.65 (CH_2 in mPEG $_{43}$), 1.24 (CH_3 in polycarbonate chain). ^{13}C NMR (600 MHz, CDCl_3 , δ , ppm): 171.83, 154.27, 135.30, 128.51, 128.16, 127.87, 70.49, 68.51, 67.08, 46.49, 17.43. The DP^{NMR} of mPEG $_{43}$ -*b*-PMBC = 40.

Synthesis of mPEG $_{43}$ -*b*-PMCC $_{40}$. mPEG $_{43}$ -*b*-PMBC $_{40}$ (20.0 g), 10% Pd/C (1.0 g), Pd(OH) $_2$ /C (1.0 g) and methanol/THF (300 mL, 1:1) were added to a 500-mL three neck flask with a magnetic stir bar under an argon atmosphere. The reaction mixture was stirred for 48 h at 35 °C under a hydrogen gas pressure system. The Pd/C and Pd(OH) $_2$ /C were filtered off, the filtrate was evaporated to dryness. The product was dried under vacuum until a constant sample mass was obtained. FT-IR (KBr, cm^{-1}): 3600–2500 (–COOH); 1753 (C=O); 1251, 1145 (C–O–C). ^1H NMR (600 MHz, CDCl_3 , δ , ppm): 4.19 (CH_2 in polycarbonate chain), 3.50 (CH_2 in mPEG $_{43}$), 1.14 (CH_3 in polycarbonate chain). ^{13}C NMR (600 MHz, DMSO, δ , ppm): 173.91, 154.45, 70.16, 69.23, 46.02, 17.36.

Synthesis of mPEG $_{43}$ -PMCC $_{25}$ -P(MCC–DHO) $_{15}$. In a 250-mL three-neck flask with magnetic stir bar, mPEG $_{43}$ -*b*-PMCC $_{40}$ (4.98 g), *N,N'*-dicyclohexyl carbodiimide (DCC) (5.95 g), and *N,N'*-dimethylaminopyridine (DMAP) (0.60 g) were dissolved in 100 mL of THF. DHO (14.9 g, 28.9 mmol) dissolved in 50 mL of THF was added dropwise to the above mixture. The reaction mixture was stirred for 48 h at 30 °C. The resulting mixture was washed with deionized water, and frozen at –20 °C for 15 min, then a solid, *N,N'*-dicyclohexyl urea, was precipitated by high speed centrifuge and filtered off. The filtrate was dried with anhydrous MgSO_4 , filtered and evaporated to dryness. The crude product was purified by dissolving it in dichloromethane and precipitated in ice-cold methanol, and then dried in a vacuum until a constant sample mass was obtained. $M_n^{\text{NMR}} = 15,755$ Da; $M_n^{\text{GPC,THF}} = 12,789$ g/mol; $\text{PDI}^{\text{THF}} = 1.69$. FT-IR (KBr, cm^{-1}): 2931, 2857 (CH_3 –, – CH_2 –), 1754 (C=O), 1248, 1143 (C–O–C). ^1H NMR (600 MHz, CDCl_3 , δ , ppm): ^1H NMR (δ , ppm from TMS in CDCl_3): $\delta = 5.34$ (t, – $\text{CH}=\text{C}$ <), 4.40 (q, > CHO –), 4.29 (m, CH_2 in polycarbonate chain), 4.12 (m, $\text{O}=\text{COCH}_2$ –), 3.65 (t, CH_2 in mPEG $_{43}$), 3.47–3.38 (m, –(CH_2) $_5$ CH_2O – and – OCH_2CH <), 3.12 [m, –(CH_2) $_6$ OCH <], 2.36 [(m, $\text{OCH}_2\text{CH}_2\text{C}(\text{CH}_2)=\text{CH}$ – (eq)], 2.19 [m, > $\text{C}=\text{CHCH}_2\text{CH}$ < (eq)], 1.23 (CH_3 in polycarbonate chain), 1.02 [s, – $\text{HC}=\text{C}(\text{CH}_2)\text{C}(\text{CH}_2)_2\text{CH}_3$], 0.98 [d, – $\text{CH}(\text{CH}<)\text{CH}_3$], 0.79 [m, – $\text{C}(\text{CH}_2)$ –($\text{CH}<)\text{CH}_3$ and $\text{OCH}_2\text{CH}(\text{CH}_2)\text{CH}_3$], 2.03–1.30 (rest of protons from diosgenyl). ^{13}C NMR (600 MHz, DMSO, δ , ppm): 172.50, 154.32, 141.05, 121.06, 109.21, 80.74, 78.83, 70.47, 68.49, 67.86, 66.75, 65.38, 62.01, 56.44, 52.45, 50.04, 46.39, 41.51, 40.18, 39.70, 39.08, 37.17, 36.96, 33.83, 32.63, 32.01, 31.76, 31.32, 30.21, 30.03, 29.61, 28.71, 25.96, 20.76, 19.32, 17.38, 17.05, 16.20, 14.44.

Self-assembly of mPEG $_{43}$ -PMCC $_{25}$ -P(MCC–DHO) $_{15}$. The copolymer (5.0 mg) was dissolved in THF (5.0 mL), then the polymer solution in THF was transferred to a prewashed dialysis membrane with a molecular weight cutoff (MWCO) of 3500 Da (Spectra/Por) and was dialyzed at room temperature against water (1.5 L) with different pH (2.0–10.0), the pH controlled by HCl or ammonium hydroxide, and the water changed at 6, 12, and 24 h. Typically the final concentration of the polymer solution after dialysis was about 0.6 mg/mL.

4. Conclusions

In summary, a new amphipathic chiral LC polycarbonate containing side diosgenyl groups was successfully synthesized. The amphiphilic block copolymers mPEG $_{43}$ -PMCC $_{25}$ -P(MCC–DHO) $_{15}$ could exhibit an LC state below body temperature and have unique self-assembly behaviors in aqueous solution, both in sphere micelles (pH < 7.0) and fiber-like micelles (pH \geq 7.0). This is an important result for potential applications taking advantage of these different morphologies. In addition, the chiral LC polymers studied here are based on entirely biocompatible diosgenyl mesogens. Our target is using the system to design drug carriers for future applications. It remains a challenge to establish how to control the polymer morphology transition precisely at different pH values, which will be a main subject of further study.

Supplementary Materials: The following are available online at <http://www.mdpi.com/2079-4991/7/7/169/s1>, Figure S1: ^1H NMR spectra of MBC, Figure S2: ^1H NMR spectra of mPEG $_{43}$ -*b*-PMBC $_{40}$, Figure S3: FT-IR

spectroscopy of copolymers, Figure S4: GPC profiles (THF as an eluent, 1 mL/min) of mPEG₄₃-b-PMBC₄₀, Figure S5: ¹H NMR spectra of mPEG₄₃-b-PMCC₄₀, Figure S6: TEM images of mPEG₄₃-PMCC₂₅-P(MCC-DHO)₁₅ self-assembly obtained in water at (A) pH = 6 and (B) pH = 8.

Acknowledgments: This work was supported by the National Natural Science Foundation of China (51503093), Fundamental Research Funds for the Central Universities (N160504001, N160503001), the National Key Research and Development Program of China (2016YFC1000902).

Author Contributions: Jian-She Hu and Li-Qun Yang conceived and designed the experiments; Zhi-Hao Guo performed the experiments, analyzed the data and wrote the paper draft; Zhang-Pei Chen help to analyze compounds structures; Xiao-Feng Liu help to perform the POM test.

Conflicts of Interest: The authors declare no conflict of interest.

References

1. Surnar, B.; Jayakannan, M. Stimuli-responsive poly (caprolactone) vesicles for dual drug delivery under the gastrointestinal tract. *Biomacromolecules* **2013**, *14*, 4377–4387. [[CrossRef](#)] [[PubMed](#)]
2. Venkataraman, S.; Lee, A.L.; Maune, H.T. Formation of disk-and stacked-disk-like self-assembled morphologies from cholesterol-functionalized amphiphilic polycarbonate diblock copolymers. *Macromolecules* **2013**, *46*, 4839–4846. [[CrossRef](#)]
3. Piñol, R.; Jia, L.; Gubellini, F. Self-assembly of PEG-b-liquid crystal polymer: The role of smectic order in the formation of nanofibers. *Macromolecules* **2007**, *40*, 5625–5627. [[CrossRef](#)]
4. Jia, L.; Cao, A.; Lévy, D. Smectic polymer vesicles. *Soft Matter* **2009**, *5*, 3446–3451. [[CrossRef](#)]
5. McKenzie, B.E.; Nudelman, F.; Bomans, P.H. Temperature-responsive nanospheres with bicontinuous internal structures from a semicrystalline amphiphilic block copolymer. *J. Am. Chem. Soc.* **2010**, *132*, 10256–10259. [[CrossRef](#)] [[PubMed](#)]
6. Wang, Y.J.; Dong, C.M. Bioreducible and core-crosslinked hybrid micelles from trimethoxysilyl-ended poly (ε-caprolactone)-S-S-poly (ethylene oxide) block copolymers: Thiol-ene click synthesis and properties. *J. Polym. Sci. Part A Polym. Chem.* **2012**, *50*, 1645–1656. [[CrossRef](#)]
7. Liu, Y.; Yu, C.; Jin, H. A supramolecular Janus hyperbranched polymer and its photoresponsive self-assembly of vesicles with narrow size distribution. *J. Am. Chem. Soc.* **2013**, *135*, 4765–4770. [[CrossRef](#)] [[PubMed](#)]
8. Pang, X.; Zhao, L.; Akinc, M. Novel amphiphilic multi-arm, star-like block copolymers as unimolecular micelles. *Macromolecules* **2011**, *44*, 3746–3752. [[CrossRef](#)]
9. Piyapakorn, P.; Akagi, T.; Hachisuka, M. Structural Analysis of Unimer Nanoparticles Composed of Hydrophobized Poly (amino acid) s. *Macromolecules* **2013**, *46*, 6187–6194. [[CrossRef](#)]
10. He, J.; Huang, X.; Li, Y.C. Self-assembly of amphiphilic plasmonic micelle-like nanoparticles in selective solvents. *J. Am. Chem. Soc.* **2013**, *135*, 7974–7984. [[CrossRef](#)] [[PubMed](#)]
11. Hao, J.; Cheng, Y.; Ranatunga, R.U. A combined experimental and computational study of the substituent effect on micellar behavior of γ-substituted thermo-responsive amphiphilic poly (ε-caprolactone) s. *Macromolecules* **2013**, *46*, 4829–4838. [[CrossRef](#)]
12. Sun, L.; Petzetakis, N.; Pitto-Barry, A. Tuning the size of cylindrical micelles from poly (L-lactide)-b-poly (acrylic acid) diblock copolymers based on crystallization-driven self-assembly. *Macromolecules* **2013**, *46*, 9074–9082. [[CrossRef](#)]
13. Glavas, L.; Olsén, P.; Odellius, K. Achieving micelle control through core crystallinity. *Biomacromolecules* **2013**, *14*, 4150–4156. [[CrossRef](#)] [[PubMed](#)]
14. Li, Y.; Akiba, I.; Harrisson, S. Facile Formation of Uniform Shell-Crosslinked Nanoparticles with Built-in Functionalities from N-Hydroxysuccinimide-Activated Amphiphilic Block Copolymers. *Adv. Funct. Mater.* **2008**, *18*, 551–559. [[CrossRef](#)]
15. Chang, H.Y.; Lin, Y.L.; Sheng, Y.J. Structural Characteristics and Fusion Pathways of Onion-Like Multilayered Polymersome Formed by Amphiphilic Comb-Like Graft Copolymers. *Macromolecules* **2013**, *46*, 5644–5656. [[CrossRef](#)]
16. Ray, J.G.; Naik, S.S.; Hoff, E.A. Stimuli-Responsive Peptide-Based ABA-Triblock Copolymers: Unique Morphology Transitions With pH. *Macromol. Rapid Commun.* **2012**, *33*, 819–826. [[CrossRef](#)] [[PubMed](#)]
17. Chen, D.; Luo, Z.; Li, N. Amphiphilic polymeric nanocarriers with luminescent gold nanoclusters for concurrent bioimaging and controlled drug release. *Adv. Funct. Mater.* **2013**, *23*, 4324–4331. [[CrossRef](#)]

18. Shen, J.; Chen, C.; Fu, W. Conformation-specific self-assembly of thermo-responsive poly (ethylene glycol)-b-polypeptide diblock copolymer. *Langmuir* **2013**, *29*, 6271–6278. [[CrossRef](#)] [[PubMed](#)]
19. Korchagina, E.V.; Qiu, X.P.; Winnik, F.M. Effect of heating rate on the pathway for vesicle formation in salt-free aqueous solutions of thermosensitive cationic diblock copolymers. *Macromolecules* **2013**, *46*, 2341–2351. [[CrossRef](#)]
20. Zhao, J.; Jeromenok, J.; Weber, J. Thermoresponsive aggregation behavior of triterpene-poly (ethylene oxide) conjugates in water. *Macromol. Biosci.* **2012**, *12*, 1272–1278. [[CrossRef](#)] [[PubMed](#)]
21. Xiang, F.; Stuart, M.; Vorenkamp, J. One-Pot Synthesis for Biocompatible Amphiphilic Hyperbranched Polyurea Micelles. *Macromolecules* **2013**, *46*, 4418–4425. [[CrossRef](#)]
22. Das, A.; Ghosh, S. Luminescent invertible polymersome by remarkably stable supramolecular assembly of naphthalene diimide (NDI) π -system. *Macromolecules* **2013**, *46*, 3939–3949. [[CrossRef](#)]
23. Lee, C.H.; Wong, C.H.; Ouhab, D. Synthesis and characterization of solvent-invertible amphiphilic hollow particles. *Langmuir* **2013**, *29*, 7583–7590. [[CrossRef](#)] [[PubMed](#)]
24. Hevus, I.; Modgil, A.; Daniels, J. Invertible micellar polymer assemblies for delivery of poorly water-soluble drugs. *Biomacromolecules* **2012**, *13*, 2537–2545. [[CrossRef](#)] [[PubMed](#)]
25. Hoffman, A.S.; Stayton, P.S.; El-Sayed, M.E.H. Design of “Smart” Nano-Scale Delivery Systems for Biomolecular Therapeutics. *J. Biomed. Nanotechnol.* **2007**, *3*, 213–217. [[CrossRef](#)]
26. Hoffman, A.S. Stimuli-responsive polymers: Biomedical applications and challenges for clinical translation. *Adv. Drug Deliv. Rev.* **2013**, *65*, 10–16. [[CrossRef](#)] [[PubMed](#)]
27. Liu, X.F.; Zhang, X.N.; Song, Z.W. Study on new chiral liquid crystalline monomers and polymers containing menthyl groups. *Liq. Cryst.* **2014**, *41*, 986–999. [[CrossRef](#)]
28. Hwang, J.J.; Iyer, S.N.; Li, L.S. Self-assembling biomaterials: liquid crystal phases of cholesteryl oligo (L-lactic acid) and their interactions with cells. *Proc. Natl. Acad. Sci. USA* **2002**, *99*, 9662–9667. [[CrossRef](#)] [[PubMed](#)]
29. Guo, J.; Sun, J.; Cao, H. Synthesis and characterization of functionalized triblock polymer: The prepared polymer is cholesteryl terminated and chain-extended PCL. *J. Appl. Polym. Sci.* **2007**, *105*, 3505–3512. [[CrossRef](#)]
30. Wan, T.; Zou, T.; Cheng, S.X. Synthesis and characterization of biodegradable cholesteryl end-capped polycarbonates. *Biomacromolecules* **2005**, *6*, 524–529. [[CrossRef](#)] [[PubMed](#)]
31. Ercole, F.; Whittaker, M.R.; Quinn, J.F. Cholesterol modified self-assemblies and their application to nanomedicine. *Biomacromolecules* **2015**, *16*, 1886–1914. [[CrossRef](#)] [[PubMed](#)]
32. Sato, K.; Fujita, S.; Iemitsu, M. Acute administration of diosgenin or dioscorea improves hyperglycemia with increases muscular steroidogenesis in STZ-induced type 1 diabetic rats. *J. Steroid Biochem.* **2014**, *143*, 152–159. [[CrossRef](#)] [[PubMed](#)]
33. Iglesias-Arteaga, M.A.; Sandoval-Ramírez, J.; Mata-Esma, M.Y. Abnormal Beckmann rearrangement in 23-hydroxyiminodiosgenin acetate. *Tetrahedron Lett.* **2004**, *45*, 4921–4926. [[CrossRef](#)]
34. Man, S.; Gao, W.; Zhang, Y. Chemical study and medical application of saponins as anti-cancer agents. *Fitoterapia* **2010**, *81*, 703–714. [[CrossRef](#)] [[PubMed](#)]
35. Ribeiro, M.H. Naringinases: Occurrence, characteristics, and applications. *Appl. Microbiol. Biot.* **2011**, *90*, 1883–1895. [[CrossRef](#)] [[PubMed](#)]
36. Wang, Y.J.; Pan, K.L.; Hsieh, T.C. Diosgenin, a plant-derived sapogenin, exhibits antiviral activity in vitro against hepatitis C virus. *J. Nat. Prod.* **2011**, *74*, 580–584. [[CrossRef](#)] [[PubMed](#)]
37. Ku, C.M.; Lin, J.Y. Anti-inflammatory effects of 27 selected terpenoid compounds tested through modulating Th1/Th2 cytokine secretion profiles using murine primary splenocytes. *Food Chem.* **2013**, *141*, 1104–1113. [[CrossRef](#)] [[PubMed](#)]
38. Gong, G.; Qin, Y.; Huang, W. Anti-thrombosis effect of diosgenin extract from dioscorea zingiberensis CH Wright in vitro and in vivo. *Phytomedicine* **2011**, *18*, 458–463. [[CrossRef](#)] [[PubMed](#)]
39. Jan, T.R.; Wey, S.P.; Kuan, C.C. Diosgenin, a steroidal sapogenin, enhances antigen-specific IgG2a and interferon- γ expression in ovalbumin-sensitized BALB/c mice. *Planta Med.* **2007**, *53*, 421–426. [[CrossRef](#)] [[PubMed](#)]
40. Yang, J.S.; Wu, C.C.; Kuo, C.L. Solanum lyratum Extracts Induce Extrinsic and Intrinsic Pathways of Apoptosis in WEHI-3 Murine Leukemia Cells and Inhibit Allograft Tumor. *Evid. Based Complement. Altern. Med.* **2012**, *2012*, 254960. [[CrossRef](#)] [[PubMed](#)]

41. Lee, A.L.; Venkataraman, S.; Sirat, S.B. The use of cholesterol-containing biodegradable block copolymers to exploit hydrophobic interactions for the delivery of anticancer drugs. *Biomaterials* **2012**, *33*, 1921–1928. [[CrossRef](#)] [[PubMed](#)]
42. Pangeni, R.; Sahni, J.K.; Ali, J. Resveratrol: Review on therapeutic potential and recent advances in drug delivery. *Expert Opin. Drug Deliv.* **2014**, *11*, 1285–1298. [[CrossRef](#)] [[PubMed](#)]
43. Xie, Y.; Hu, J.; Dou, Q. Synthesis and mesomorphism of new aliphatic polycarbonates containing side cholesteryl groups. *Liq. Cryst.* **2016**, *43*, 1486–1494. [[CrossRef](#)]
44. Wang, Y.; Li, Q. Light-Driven Chiral Molecular Switches or Motors in Liquid Crystals. *Adv. Mater.* **2012**, *24*, 1926–1945. [[CrossRef](#)] [[PubMed](#)]
45. Wang, L.; Li, Q. Stimuli-Directing Self-Organized 3D Liquid-Crystalline Nanostructures: From Materials Design to Photonic Applications. *Adv. Funct. Mater.* **2016**, *26*, 10–28. [[CrossRef](#)]
46. Tangso, K.J.; Patel, H.; Lindberg, S. Controlling the Mesostructure Formation within the Shell of Novel Cubic/Hexagonal Phase Cetyltrimethylammonium Bromide–Poly (acrylamide-acrylic acid) Capsules for pH Stimulated Release. *ACS Appl. Mater. Interfaces* **2015**, *7*, 24501–24509. [[CrossRef](#)] [[PubMed](#)]
47. Negrini, R.; Mezzenga, R. pH-responsive lyotropic liquid crystals for controlled drug delivery. *Langmuir* **2011**, *27*, 5296–5303. [[CrossRef](#)] [[PubMed](#)]



© 2017 by the authors. Licensee MDPI, Basel, Switzerland. This article is an open access article distributed under the terms and conditions of the Creative Commons Attribution (CC BY) license (<http://creativecommons.org/licenses/by/4.0/>).